GRAIN FRICTION CONTROLS CHARACTERISTICS OF SEISMIC CYCLE IN GRANULAR FAULT GOUGE; IMPLICATIONS FOR FAULT PARTICLE ROUGHNESS

Authors:

I. Omid Dorostkar[1,2,*]

1. Chair of Building Physics, Department of Mechanical and Process Engineering, Swiss Federal Institute of Technology Zurich (ETH Zurich), Stefano-Franscini-Platz 5, CH-8093 Zurich, Switzerland
2. Department of Civil, Environmental and Geomatic Engineering, Swiss Federal Institute of Technology Zurich (ETH Zurich), Stefano-Franscini-Platz 5, CH-8093 Zurich, Switzerland

*Corresponding author:

Email: domid@ethz.ch Phone: +41587654106

ID: orcid.org/0000-0002-7758-4919

II. Jan Carmeliet[1]

1. Chair of Building Physics, Department of Mechanical and Process Engineering, Swiss Federal Institute of Technology Zurich (ETH Zurich), Stefano-Franscini-Platz 5, CH-8093 Zurich, Switzerland

Email: cajan@ethz.ch

Abstract:

In this paper, we study the effect of particle roughness approximated by the inter-particle friction coefficient on the characteristics of seismic cycles. Our discrete element simulations show that the stick-slip frictional strength and dilation of the fault gouge, as well as their variability, nonlinearly increase with the particle roughness (inter-particle friction coefficient) but at high particle roughness saturate. By statistical analyses on a large number of slip events, we find that the average recurrence time and its variability decreases with particle roughness. A rougher fault shows a more complex nucleation phase and more frequent energy releases in the kinetic energy signal. We find that the rougher fault on average shows more small slip events compared to smoother fault but also contains a limited number of extreme events. The fault gouge with higher particle surface roughness shows higher stored potential energy and stronger particle-particle contact forces. Our pseudo acoustic emission analysis, based on the monitoring of the velocity signal of particles, shows higher temporal and more spatially distributed acoustic emissions for fault gouge with higher particle surface roughness. Our findings in this study show that roughness at micro-scale plays an important role in nucleation and rupture process of earthquakes, similar to conditions where no granular gouge was considered. Our results in this study are consistent with previous numerical and experimental works and complete them by focusing on micromechanics of fault damage zone, showing how numerical models and in particular discrete element simulations can help enhance our understanding from fault mechanics.

Keywords: friction, roughness, stick-slip, granular materials, fault gouge, fault mechanics

1- Introduction

The stability and slip behavior of natural faults and their relation with fault properties and in particular, their surface roughness, have been under debate during last years. The fault roughness spans from microns to tens of kilometers and can be measured using different methods. Brodsky et al. [2016] quantified the slip surface roughness and found that fault surface is rougher at small scales than large ones and that the scale dependence of roughness implies yielding of asperities at all scales [*Brodsky et al., 2016*]. Using three independent scanner devices, Candela et al. [2012] characterized the roughness of fault surfaces by a single anisotropic self-affine description [*Candela et al., 2012*]. The fault surface roughness has been evaluated also by measurements on exhumed faults [*Renard et al., 2006; Sagy et al., 2007; Candela et al., 2009; Bistacchi et al., 2011; Brodsky et al., 2011*].

At field scale, the fault roughness is suggested to control the stress drop and slip distribution during earthquakes [*Bouchon et al., 2010; Candela et al., 2011a; Candela et al., 2011b*]. The maturity and roughness level of nearby faults are also reported to influence seismic hazard associated with hydraulic fracturing [*Kozłowska et al., 2018*]. A recent report shows that the seafloor in front of large earthquakes is generally smoother than in areas where no large earthquakes have occurred [*Rijsingen et al., 2018*]. In their review paper on field scale observation regarding fault creep caused by subduction of rough seafloor relief, Wang & Bilek [2014] reported lack of evidence for rough faults to be more strongly locked, while creeping is observed for both smooth and rough faults [*Wang & Bilek, 2014*].

It is barely feasible to study the relation of roughness and seismicity in nature. At lab scale, experimental studies showed that roughness promotes a larger nucleation segment [*Ohnaka & Shen, 1999; Ohnaka, 2003*]. The study by Goebel et al. [2014] showed that, as the shearing of an experimental sample advances, there exists a rapid spatial decay of acoustic emission events during following inter-slip periods, that is an intimation of decreasing fault zone complexity and fault surface roughness [*Goebel et al., 2014a*]. In experiments, the smoother faults are proposed to show super-shear ruptures as roughness controls the velocity of rupture propagation [*Xia et al., 2004; Schubnel et al., 2011*]. The topology and fault structure influence the spatial and temporal distribution of small and large earthquakes. Using laboratory experiments, Goebel et al. [2017] showed that more mature, smoother faults produce localized seismicity, smoother stress fields, and lower b-values (the measure for the relative abundance of the strong to the weak earthquakes based on the Gutenberg–Richter law), and that the acoustic emission statistics during stick-slip are strongly influenced by fault roughness [*Goebel et al., 2017*]. In their recent review on scaling of fault roughness and its implications for earthquake mechanics, Renard & Candela [2017] emphasized on the open question of fault roughness at small scales (below the millimeter scale) and its possible implications for seismic and aseismic slip [*Renard & Candela, 2017*].

Numerical simulations have been also used to study the effect of roughness on mechanics and nucleation of slip events as well as heterogeneity of stress distribution and dissipation due to fault zone roughness [*Chester & Chester, 2000; Dieterich & Smith,* *2009; Angheluta et al., 2011; Dunham et al., 2011; Bruhat et al., 2016; Tal & Hager, 2018; Tal et al., 2018*]. Previous research using 2-D discrete element method (DEM) showed that the fault roughness can control the slip style from stick-slip to stable sliding [*Fournier & Morgan, 2012*]. Using 3-D DEM, Rathbun et al. [2013] found that, in stable sliding regime, roughness and thus coupling of a fault to the gouge zones influences the number of sliding contacts controlling the critical slip distance [*Marone & Kilgore, 1993; Rathbun et al., 2013*]. Using large-scale numerical simulations, Zielke et. al [2017] suggested that, besides stress drop and rupture dimension, the earthquake moment release and its recurrence probability is dependent also on surface roughness [*Zielke et al., 2017*]. In a new numerical study, Pierre et al. [2018] showed, without appealing to complex friction rheology, that a simple geometrical complexity with two overlapping faults give rise to both slow and fast slip events [*Pierre et al., 2018*].

Faults at their core are usually characterized by a granular gouge layer created by wear, communition and other frictional processes, as observed in nature [*Engelder, 1974; Shimamoto, 1979; Chester et al., 1985; Chester & Logan, 1986; Marone et al., 1990; Chester & Chester, 1998; Cashman & Cashman, 2000; Chester & Chester, 2000; Faulkner et al., 2003; Heermance et al., 2003; Cashman et al., 2007; Zoback et al., 2010*]. Characteristics of slip events in laboratory stick-slip experiments including stress drop, pre-seismic friction, recurrence time, granular layer compaction etc. have been studied widely for different loading configurations and particle properties [*Dieterich & Kilgore, 1994; Marone, 1998a; Karner & Marone, 2000; Mair et al., 2002; Brantut et al.,* *2008; Rathbun & Marone, 2010; Haines et al., 2014; Rosenau et al., 2017*], where the frictional strength and stability of a sheared granular zone are found sensitive to grain shape, particle size distribution and their evolution [*Mair et al., 2002; Anthony & Marone, 2005*].

Despite its dependency on many factors, generally the contact friction coefficient increases with surface roughness parameters [*Biegel et al., 1989; Ivković et al., 2000; Park & Song, 2009*]. In this study, we systematically vary the inter-particle friction coefficient as a proxy for particle roughness in a granular fault gouge, as the presence of granular fault gouge is neglected in most of the previous studies on fault roughness. We focus on stick-slip dynamics and the effect of particle roughness on characteristics of seismic cycles to answer the following question; "what is the effect of inter-particle roughness on the slip size distribution and inter-event time of seismic cycles in a fault with granular fault gouge?". To this end, we perform 3-D DEM simulations recording hundreds of slip events for statistical analyses provided by the advantage of numerical simulations. We also study the evolution of elastic strain energy (potential energy [*Dorostkar, 2018; Dorostkar & Carmeliet, 2018*]), kinetic energy, and the micromechanics of slip events and explain the macro-scale response of fault with grain-scale metrics (e.g. [*Dorostkar et al., 2017a*]). In absence of complex rheological and geometrical granular contact model, we will show that, although our simplified numerical approach does not contain many complexities present in nature, it can yet show similar observations to recent numerical and experimental studies on fault roughness and complete them by statistical analyses using a large quantity of slip events. Our findings in this study will show that roughness at micro-scale level, approximated by inter-particle friction coefficient, may play a similar role in mechanics of earthquakes as roughness of fault blocks' surface in absence of fault gouge.

2- Model description

Due to particulate nature of granular fault gouge, we use DEM to model gouge grains. In DEM, the equations of motion solved for each particle considering the applied forces are:

$$\sum F_p = m(\frac{d}{dt} u_p), \tag{1}$$

$$\sum T_p = I(\frac{d}{dt} \omega_p), \tag{2}$$

where m, I, u_p and ω_p are the mass, the moment of inertia and the translational and angular velocity of particle, respectively. In Eq. (1) and (2), F_p and T_p are the forces and torques acting on particle *i* owing to particle-particle contacts. In soft sphere DEM, the particle-particle contact allows an overlap between them and the contact law is described by a combination of different rheological elements (spring, dashpot, slider etc.). These elements are at play when particles are in contact. Upon contact loss, there are no contact forces acting between the particles. The process of forming new contacts and contact loss changes the stiffness of the granular system. Particle sliding also changes the shear stiffness. These phenomena introduce a nonlinear strain dependent behavior of the granular material [*O'Sullivan, 2011*]. The contact nonlinearity is mainly effective at smaller strains, while material nonlinearity arises mainly from a change in the number and the fabric of contacts taking place at larger strains [*O'Sullivan, 2011*]. Material nonlinearity is recognized to play an important role in the weakening process of granular materials [*Johnson & Jia, 2005*]. There is a variety of contact laws used in DEM [*Di Renzo & Di Maio, 2004*], however, in order to capture particle scale nonlinearity, we use the nonlinear Hertzian contact law. In this particle-particle contact law, the spring stiffness and the coefficient of damping are function of particle material properties and the overlap between particles [*Hertz, 1882; Di Renzo & Di Maio, 2004*]. The normal and tangential contact forces are calculated as follows:

$$F_{pn} = -k_{pn}\delta\varepsilon_{pn} + c_{pn}\delta u_{pn} \,, \tag{3}$$

$$F_{pt} = \min\left\{\left|k_{pt}\int_{t_{c,0}}^{t}\delta u_{pt}\,dt + c_{pt}\delta u_{pt}\right|, \mu_c F_{pn}\right\}, \tag{4}$$

where k_{pn} and k_{pt} are the normal and tangential spring stiffness, c_{pn} and c_{pt} are the normal and tangential damping coefficient, $\delta\varepsilon_{pn}$ is the overlap and δu_{pn} and δu_{pt} are the relative normal and tangential velocities of two particles in contact, respectively. In Eq. (4), the parameter μ_c represents the inter-particle friction coefficient that limits the tangential force. When the tangential contact force between two particles in contact reaches this limit, they start sliding against each other. The integral term in Eq. (4) shows an incremental spring, storing energy based on the relative elastic tangential deformation of the particle surface starting from the moment particles touch each other at $t_{c,0}$. A damping is added to the spring component of the tangential force if the Coulomb criterion is not met [*Di Renzo &*

Di Maio, 2004; Goniva et al., 2012]. The spring and damping coefficients are calculated as follows:

$$k_{pn} = \frac{4}{3} Y^* \sqrt{R^* \delta \varepsilon_{pn}} \,, \tag{5}$$

$$k_{pt} = 8\, G^* \sqrt{R^* \delta \varepsilon_{pn}} \,, \tag{6}$$

$$c_{pn} = -2 \sqrt{\frac{5}{6}} \times \frac{\ln(r)}{\sqrt{ln^2(r) + \pi^2}} \times \sqrt{2 Y^* \sqrt{R^* \delta \varepsilon_{pn}}\, m^*} \,, \tag{7}$$

$$c_{pt} = -2 \sqrt{\frac{5}{6}} \times \frac{\ln(r)}{\sqrt{ln^2(r) + \pi^2}} \times \sqrt{8\, G^* \sqrt{R^* \delta \varepsilon_{pn}} m^*} \,, \tag{8}$$

where, r is the restitution coefficient, and Y^*, R^*, G^* and m^* are the equivalent Young's modulus , radius, shear modulus and mass, respectively, calculated as follows:

$$\frac{1}{Y^*} = \frac{(1-\upsilon_1^2)}{Y_1} + \frac{(1-\upsilon_2^2)}{Y_2} \,, \tag{9}$$

$$\frac{1}{G^*} = \frac{2(2-\nu_1)(1+\nu_1)}{Y_1} + \frac{2(2-\nu_2)(1+\nu_2)}{Y_2} \,, \tag{10}$$

$$\frac{1}{R^*} = \frac{1}{R_1} + \frac{1}{R_2} \,, \tag{11}$$

$$\frac{1}{m^*} = \frac{1}{m_1} + \frac{1}{m_2} \,, \tag{12}$$

where subscripts 1 and 2 refer to the two particles in contact and υ is the Poisson's ratio of the particle.

Figure 1 illustrates a granular layer representing a part of a granular fault gouge. In our model, 8000 spherical particles constitute this layer with particle diameter ranging 90-150 μm having a uniform, poly-disperse particle size distribution. The sample size in our simulations is 11×1.5×0.8 mm^3. This sample size is large enough to show proper effect of 3D particle interaction [*Ferdowsi, 2014*] as well as jamming/unjamming transitions in the granular layer [*Marone et al., 2008*]. On the sample top and bottom, we employ two corrugated plates with high surface roughness modeled by a friction coefficient of 0.9 between the plates and particles to facilitate the transmission of shear stresses to the granular gouge. This kind of geometry is inspired from the BIAX laboratory earthquake machine using corrugated driving blocks [*Marone, 1998a; Rivière et al., 2018*]. In this paper, our study is dedicated to influence of the particle roughness of fault gouge material represented by inter-particle friction coefficient on stick-slip behavior. We do not study the effect of characteristics of the corrugated plates e.g. length, depth, etc. on the dynamics of the sheared granular layer, since a detailed analysis showed that change of these characteristics does not alter the dynamic regime. On the front- and back-sides of the sample, we implement frictionless walls with the same elastic properties of particles. This type of interaction between particles and walls are designed to avoid rigid wall boundary conditions. Wall-particle interaction in our DEM model is the same as particle-particle interaction when one particle has an infinite radius. Periodic boundary conditions are applied at the left and right sidewalls representing a long fault gouge in x direction. The periodic boundary conditions allow for large shear displacements, and facilitate recording many slip events to be used for statistical analyses. To prepare the sample, particles are inserted randomly in space descending with an initial velocity of 10^{-2} cm/s. Next, the upper plate is moved downward to apply a confining stress to confine the sample. At this stage, the confining stress increases until the desired confining stress is attained (10 MPa). The position of the upper plate is adapted continuously, as in the lab experiments, in order to maintain the confining stress constant. At constant confining stress, shearing is initiated by moving the bottom plate in *x* direction with a displacement-controlled mechanism (constant velocity of 600 μm/s) until reaching the maximum shear stress, at which point the stick-slip process commences. The particle density is 2900 kg/m^3 that results in an applied time step for DEM calculations of 15×10^{-9} seconds, within the recommended range based on the Rayleigh time. Our DEM calculations remain in the quasi-static regime by controlling the inertial number to be below 10^{-3} [*MiDi, 2004; Sheng et al., 2004; Agnolin & Roux, 2007*]. Similar to our previous works [*Dorostkar et al., 2017c; Dorostkar et al., 2018*], we use LIGGGHTS [*Goniva et al., 2012; Kloss et al., 2012*] to model the granular fault gouge.

3- Results

We show in Fig. 2a and 2b the evolution of macroscopic friction and gouge thickness, respectively, for three different inter-particle frictions of 0.1, 0.5 and 0.9 during the stick-slip dynamics. The macroscopic friction is defined as the ratio of shear stress to normal stress (confining stress) on the driving block and the gouge thickness represents the measurement in z direction of Fig. 1. Figure 2c shows with higher resolution the shaded area in Fig. 2a. The macroscopic friction (or shear stress since the confining stress is kept constant) increases nonlinearly reaching to a critical state where micro-slips take place followed by a major slip event. The average macroscopic friction increases nonlinearly with the inter-particle friction coefficient: at low inter-particle coefficients (0.1 to 0.5), the macroscopic friction coefficient increases much more compared to high inter-particle coefficients (0.5 and 0.9). A similar behavior can be observed for the gouge thickness (Fig. 2b).

We perform long simulations for inter-particle friction coefficients between 0.1 - 1 and measure the average macroscopic friction over all stick and slip phases (Fig. 3a). We observe that the gouge strength represented by macroscopic friction increases nonlinearly with inter-particle friction and saturates at around μ_c = 0.9 to 1. A similar behavior is observed for gouge thickness (Fig. 3b). The standard deviations in macroscopic friction signal and gouge thickness are found to increase with increasing inter-particle friction coefficient (Fig. 3a and 3b). We calculate the slip recurrence time for slip events with a drop in macroscopic friction larger than 0.01, a threshold that avoids capturing micro-slips before a major slip event [*Dorostkar et al., 2017b*]. The slip recurrence time and its standard deviation decreases with increasing inter-particle friction coefficient, meaning that slip events occur more often and more regularly in a gouge with higher frictional particles (Fig. 3c)

To complement the observations in Fig. 3, in Fig. 4a, we observe an almost linear relation between macroscopic friction and gouge thickness for simulations with different inter-particle friction coefficient. The more dense population of data points at higher thickness and macroscopic friction is consistent with the nonlinear behavior observed in Figs. 2b and 2c. We also observe that the number of slip events increases with increasing inter-particle coefficient (equivalent to a decreasing recurrence time as seen in figure 3c) The histogram of slip events' friction drop (Fig. 5) shows that this increase in number of events at higher inter-particle friction coefficient mainly stems from smaller events: a fault gouge with higher inter-particle friction coefficient experiences more smaller slip events at a shorter and more regular inter-event time (less standard deviation in Fig. 3c) with lower friction (stress) drop. Remark however that, at high inter-particle friction, although the majority of the slip events are smaller, there are also some extreme slip events, which are larger than the events at lower inter-particle friction.

When studying the time evolution of the average contact force, we interestingly find a similar stick-slip type of behavior (Fig. 6). This observation shows that the macroscopic response of the sheared granular gouge is controlled by the contact forces at grain scale, i.e. by its grain scale behavior. We observe that, by increasing the inter-particle friction coefficient, the average contact force increases, however the relative increase of higher inter-particle friction coefficient becomes smaller at higher values. The decomposition of contact force into normal and tangential components shows that the contribution of the normal component is dominant irrespective of inter-particle friction coefficient. The relative contribution of normal contact force to the total contact force compared to the contribution of the tangential contact force decreases for higher inter-particle frictions. This means that, despite a small increase in tangential contact force, the overall enhanced shear strength of fault gouge (higher macroscopic friction) at higher inter-particle friction coefficient cannot solely stem from the increase of tangential contact force. In other words, although the inter-particle friction coefficient is not directly contributing to the normal contact force, its increase results in a higher normal contact force enhancing the shear capacity of the system. The hypothesis is that, there exists a structural effect where at higher inter-particle coefficient less slipping contacts occur, providing a better support for a contact network to build up higher contact forces. Indeed, when studying the slipping contact ratio (SCR), which is defined as the ratio between number of contacts at Coulomb frictional limit prone to slip and the total number of contacts, we observe drops in SCR of almost one order of magnitude when changing the inter-particle friction from 0.1 to 0.5 or from 0.5 to 0.9 (Fig. 7a). At the same time, Fig. 7b shows that the average coordination number (coordination number is the number of contacts per particle) decreases with increasing particle friction coefficient. The decrease in coordination number for higher inter-particle frictions can be attributed to the larger dilation or higher gouge thickness (see Fig. 2b). We remark that, since the coordination number decreases with increasing inter-particle friction coefficient (Fig. 7b), we also check the total number of slipping contacts that is not normalized by the number of contacts and observe similar behavior: the total number of slipping contacts decreases with increasing particle friction coefficient.

In Figs. 7c and 7d, we show the instantaneous and cumulative particle displacement averaged over all particles, respectively. The instantaneous particle displacement shows larger jumps upon micro- or major slips for higher inter-particle friction coefficients. Moreover, the cumulative particle displacement clearly shows that for a given instant in time (or a given shear strain), particles with higher inter-particle friction underwent higher total displacements. The cumulative displacement is the total displacement of a particle from the start of each simulation. Our analysis shows that particle displacement is mainly in x-direction (99 %) along the moving boundary that imposes the shear stress (Fig. 1).

We also study the evolution of potential and kinetic energies in sheared granular fault gouge (Fig. 8). The elastic strain potential energy is stored within the particle-particle contacts through overlap between particles [*Dorostkar & Carmeliet, 2018*] and the kinetic energy is due to translation and rotation of particles. The fault gouge with higher inter-particle friction coefficient shows more potential energy, however, the increase in average potential energy is not linear with the increase of inter-particle friction. For instance, an increase of friction coefficient by a factor 9, from 0.1 (Fig. 8c) to 0.9 (Fig. 8a), leads to an increase in potential energy only by a factor 3. We also observe that the kinetic energy signal for higher inter-particle frictions shows more fluctuations and bursts i.e. indicating important rearrangements of particles inside the fault gouge. While the potential energy at low inter-particle friction coefficient (Fig. 8c) shows a plateau before the major slip events, the energy is always increasing approaching slip events for higher inter-particle frictions (Fig. 8a).

We compare in Fig. 9 the evolution of macroscopic friction and gouge thickness for inter-particle friction coefficients with 2 orders of magnitude contrast i.e. 10, 1 and 0.1. The nucleation phase of slip events for higher inter-particle friction coefficient (Fig.9a) shows a complex behavior in both macroscopic friction and gouge thickness signals, where a considerable amount of small drops in friction coefficient occur during the stick phase before an upcoming extreme slip event that has a long recurrence time. The statistical analysis of the size of all slip events based on drop in macroscopic friction (Fig. 10) shows that slip events occur more often for higher inter-particle friction coefficients i.e. larger number of slip events with shorter recurrence interval. More importantly, we observe that, although the higher number of slip events stems mainly from smaller events (see also Fig. 5), there exist also some very large slip (extreme) events (Fig. 10).

A commonly used technique to monitor fault activity in experiments is Acoustic Emission (AE) [*McLaskey & Glaser, 2011; Goebel et al., 2012; Johnson et al., 2013; Goebel et al., 2014b; Goebel et al., 2017; Rivière et al., 2018*]. The origin of AE during laboratory stick-slip experiments is still under debate, where the AE is suggested to originate from groaning, creaking, and chattering of continuous grain motions and breakage of force chains within the fault gouge [*Rouet-Leduc et al., 2017; Rivière et al., 2018*]. Our analyses in this study show that the velocity (or acceleration) signal of a flagged particle demonstrates a very similar behavior to acoustic data of the lab (Fig. 11a), containing similar information for the prediction of macroscopic friction signal (e.g. [*Rouet-Leduc et al., 2017*]). However, since the velocity profile of a flagged particle contains both motion from arriving waves owing to rearrangements of other particles and the motion of the particle itself, we call it "pseudo AE" signal. In other words, although our AE signal is derived from the motion of a single, flagged particle compared to the lab signal where the AE is usually reordered with a device outside of the fault gouge; we find that the pseudo AE signal contains sufficient information for the purpose of this study, where we compare the velocity signal from the same particles for simulations with different inter-particle friction coefficient. The velocity signal shows bursts at slip events, which are larger for higher inter-particle coefficients (Fig. 11b). The complementary Cumulative Distribution Function (cCDF) of pseudo acoustic emission bursts (for all emissions without threshold, during both stick and slip phases) in Fig. 12 clearly shows the increase of AE amplitude for higher inter-particle friction coefficients. We remark that the observations in Fig. 11 and 12 are not dependent on the flagged particle and are consistently recorded for several chosen particles.

We further look at the micromechanics of fault by visualizing the particles on a plane representative of the whole box (here the front plane of the gouge) for inter-particle friction coefficients of 0.1 and 10, at a point during the stick phase (Fig. 13). For panels a and b, we set the maximum of color bar equal to the shear driving plate velocity, 0.06 cm/s. While a gradient is observed for inter-particle friction of 0.1 from top to bottom with particles close to the bottom plate having velocity close to 0.06 cm/s, the particle velocity field shows a more uniformly distributed profile for inter-particle friction of 10. We will discuss the implications of this observation in Section 4. A comparison between panels c and d shows a larger cumulative displacement for particles with inter-particle friction of 10, where the maximum of color bar is set to the maximum cumulative displacement of particles with inter-particle friction of 0.1, for a better comparison. It is clear from Fig. 13d that a larger portion of the sample has experienced a large displacement. We remind that the main displacement for particles is in x direction, along the driving plate motion. The spatial distributions in panels c and d are consistent with temporal evolution in Fig. 7d. The spatial distributions of coordination number for both inter-particle friction coefficients are rather uniform, while the gouge with lower inter-particle friction shows higher coordination numbers consistent with observations of Fig. 7b. The gouge with higher inter-particle friction shows on average lower numbers, also showing some 'blue' spots with low coordination number.

4- Discussion

We discuss our main findings and present them in the frame of comparison with other recent studies on the impact of inter-particle friction coefficient as well as fault surface roughness. The maximum macroscopic friction coefficient (or frictional strength of the sheared granular fault gouge) during stick-slip dynamics increases with inter-particle friction coefficient representing the particle roughness, but saturates at inter-particle friction values around 0.9-1 (Fig. 3). This observation is similar to previous studies on peak shear strength of granular materials as well as stable sliding of a sheared granular layer, where the nonlinear macroscopic behavior and saturation of friction are observed and attributed to rotation of particles [*J. Latham et al., 2005; Azéma et al., 2012; Shojaaee et al., 2012; Göncü & Luding, 2013; Rathbun et al., 2013; Azéma et al., 2017*]. Knuth and Marone [2007] also observed a systematic relationship between the strength of granular layers and the surface roughness of particles [Knuth & Marone, 2007]. Rough faults are suggested to undergo more deformation in the fault zone requiring more overall work to shear the fault [*Rathbun et al., 2013*], as we also observe in the higher cumulative particle displacement for fault gouge with higher particle roughness (Fig. 7 and Fig. 13). Furthermore, we show a linear relation between macroscopic stick-slip friction and gouge thickness (Fig. 4), as is confirmed by previous research [*Mead, 1925; Marone, 1998b; Frye & Marone, 2002; Knuth & Marone, 2007; Makedonska et al., 2011*].

The macroscopic frictional strength of a granular layer also follows the bulk properties (e.g. bulk stiffness) [*Rabinowicz, 1956; Knuth & Marone, 2007; Leeman et al., 2016*]. It is suggested that particle-scale roughness is responsible for enhancing the elasticity of a granular system at global scale [*Wang et al., 2007*]. Similarly, we also observe in Fig. 6 that the higher particle roughness makes a granular structure stronger, which is capable of building higher contact forces leading to a higher shear strength.

We observe higher standard deviation for both macroscopic stick-slip friction and gouge thickness with increasing roughness (Fig. 3). A hypothesis here is that the fault gouge with higher particle roughness has to undergo more complex states during deformation towards failure, which involves more locked contacts (and less slipping contacts; see Fig. 7) in spite of a lower total number of contacts, which makes the system to experience a wider range of macroscopic frictions and dilations manifested in higher variability of friction coefficient and gouge thickness (Fig. 3). The system with rougher particle surface going through those complex topographical states has to expand more to accommodate the continuous externally applied shear, which leads to a higher dilatation and a lower coordination number. These conditions make a fault gouge with rougher particle surface to fail more frequently leading to more fluctuations and variability both in macroscopic friction (slip events) and gouge thickness. Slip events in a sheared granular layer are reported as a collective phenomenon: slipping contact ratio increases approaching the failure leading to a major slip event. Therefore, from another point of view, in a system with a higher particle roughness and lower slipping contact ratio, the slip event is prevented due to stronger contacts, so that the system fails only partially leading to a large number of small slips. We also remark that, since the main displacement for particles is along the direction of the shear driving plate (x direction in Fig. 1), the higher cumulative particle displacement is consistent with a higher number of slip events, where at each slip event there is a displacement (rupture) for the center of mass of the granular fault gouge.

The recent numerical model using 2-D plane strain calculations by Tal and Hager [2018] showed that, as the roughness amplitude increases, the load in the fault is released by more slip events but with lower average stress drops [Tal & Hager, 2018]. Similarly, we observe in Fig. 4 that increase of particle roughness leads to more slip events but with lower friction drops. Using numerical simulations, Tal et al. [2018] observed a more complex behavior for faults with higher roughness, where the complexities in the nucleation process are reflected as irregular fluctuations in the moment rate for rougher faults [*Tal et al., 2018*]. Interestingly, we observe a similar complexity in 3D DEM, where the nucleation (stick) phase of slip events contains many fluctuations i.e. smaller slip events. However, using the advantage of DEM and employing the periodic boundary conditions we can, in contrast to experiments, shear the fault gouge during long time collecting information of hundreds of slip events. Using a statistical analysis, we then show that a fault gouge with high enough particle roughness and large enough shear displacement shows, besides the large amount of small events, some extreme slip events with long recurrence time compared to faults with lower roughness.

Previous research on continuous monitoring of AE during stick-slip experiments of rocks has deepened our understanding from the micromechanics of slip events [*McLaskey & Glaser, 2011; Goebel et al., 2012*]. The experimental work by Kwiatek et al. [2014] showed that the observed changes in AE characteristics are clearly correlated to the fault topography and roughness [*Kwiatek et al., 2014*]. Goebel et al. [2017] showed that faults with rougher surface show a more spatially distributed AE activity and a higher b-value [*Goebel et al., 2017*]. Our DEM simulations also show dependency of AE on fault particle roughness. We observe higher temporal (Fig. 11 and 12) and more spatially distributed AE (Fig. 13) for higher fault particle roughness. The higher AE in fault gouge with higher particle surface roughness is consistent with more frequent kinetic energy releases (Fig. 8), since AE is believed to originate from the rearrangement of particles. We remind that, although our discussion on AE is based on velocity tracking of single flagged particles (called here pseudo AE), the temporal evolution and higher moments of those signals show very similar behavior to laboratory AE (e.g. [*Rouet-Leduc et al., 2017; Rivière et al., 2018*]), as we are using them for machine learning analyses in our ongoing research.

Overall, our observations on the effect of particle roughness approximated by inter-particle friction coefficient using 3-D DEM model of a granular fault gouge show similarities to other numerical and experimental works on the effect of fault surface roughness that did not consider the granular gouge. The DEM model in this work is a vast simplification of real faults in nature but yet expands our understanding of micro-scale fault roughness and provides a mean to study and measure quantities that are not feasible to measure in the lab and in the field, showing how numerical models can boost our understanding from physical process that dictate frictional strength of a fault damage zone.

5- Conclusions

We model stick-slip dynamics of a granular fault gouge by 3-D discrete element simulations for different values of the micro-scale fault roughness (referred to as particle roughness) approximated by the inter-particle friction coefficient to better understand its effect on the characteristics of seismic cycles. The major findings of this study can be summarized as follows:

- The fault gouge frictional strength, dilation and their standard deviation nonlinearly increase with the particle roughness, saturating at high inter-particle friction.
- The average slip events' recurrence time and its standard deviation decreases with particle roughness, meaning that, rougher faults fail more frequently. A rougher fault shows a more complex nucleation (stick) phase, characterized

by many small slip events as manifested by the more frequent energy release in the kinetic energy signal.

- Our statistical analyses on a large number of slip events obtained by shearing the fault gouge to a large shear strain show that rougher faults show a higher number of slip events mainly consisting in small slip events (small drops in friction coefficient), however there are also some extreme slip events larger than the extreme events of smoother faults.
- The fault gouge with higher particle roughness shows higher stored potential energy and stronger particle-particle contacts, a structure that needs more work to deform it and therefore, for a given shear strain, the particles experience more deformation.
- The pseudo acoustic emission analysis, based on the monitoring of the velocity of particles, shows higher temporal AE for fault gouge with higher particle surface roughness.

6- Acknowledgement

The authors thank ETH Zurich for funding this study. The data related to this paper can be obtained by contacting the corresponding author at domid@ethz.ch.

7- Figures

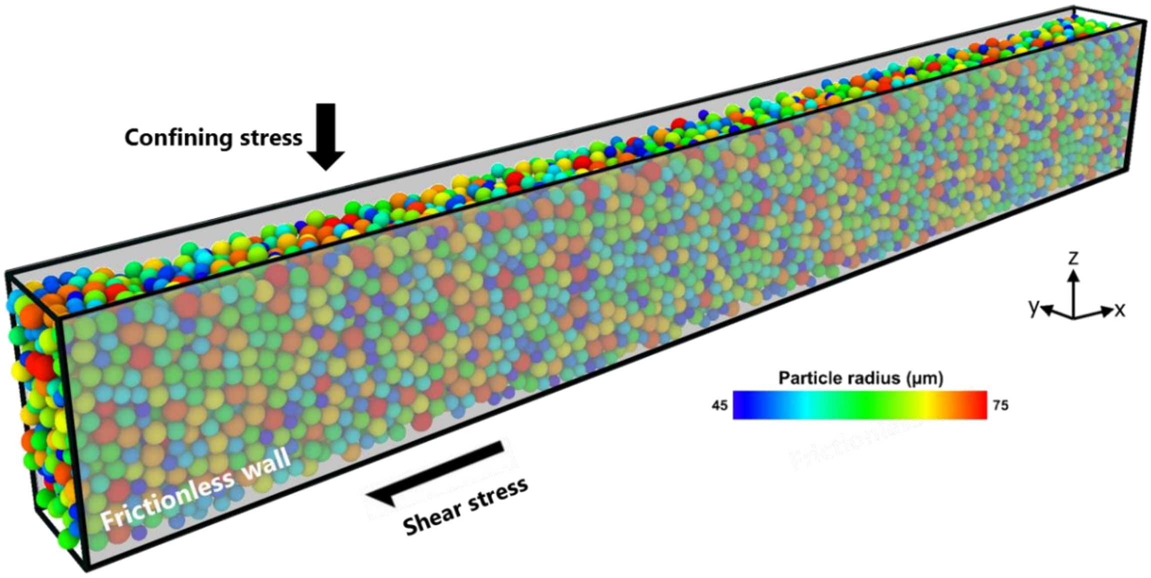

Fig. 1: Three dimensional granular fault gouge with 8000 particles with poly-disperse diameter distribution of 90-150 micrometer. The fault gouge is confined in z direction and sheared in x direction with periodic boundary conditions (Image produced with the open source visualization tool (OVITO) [Stukowski, 2010]).

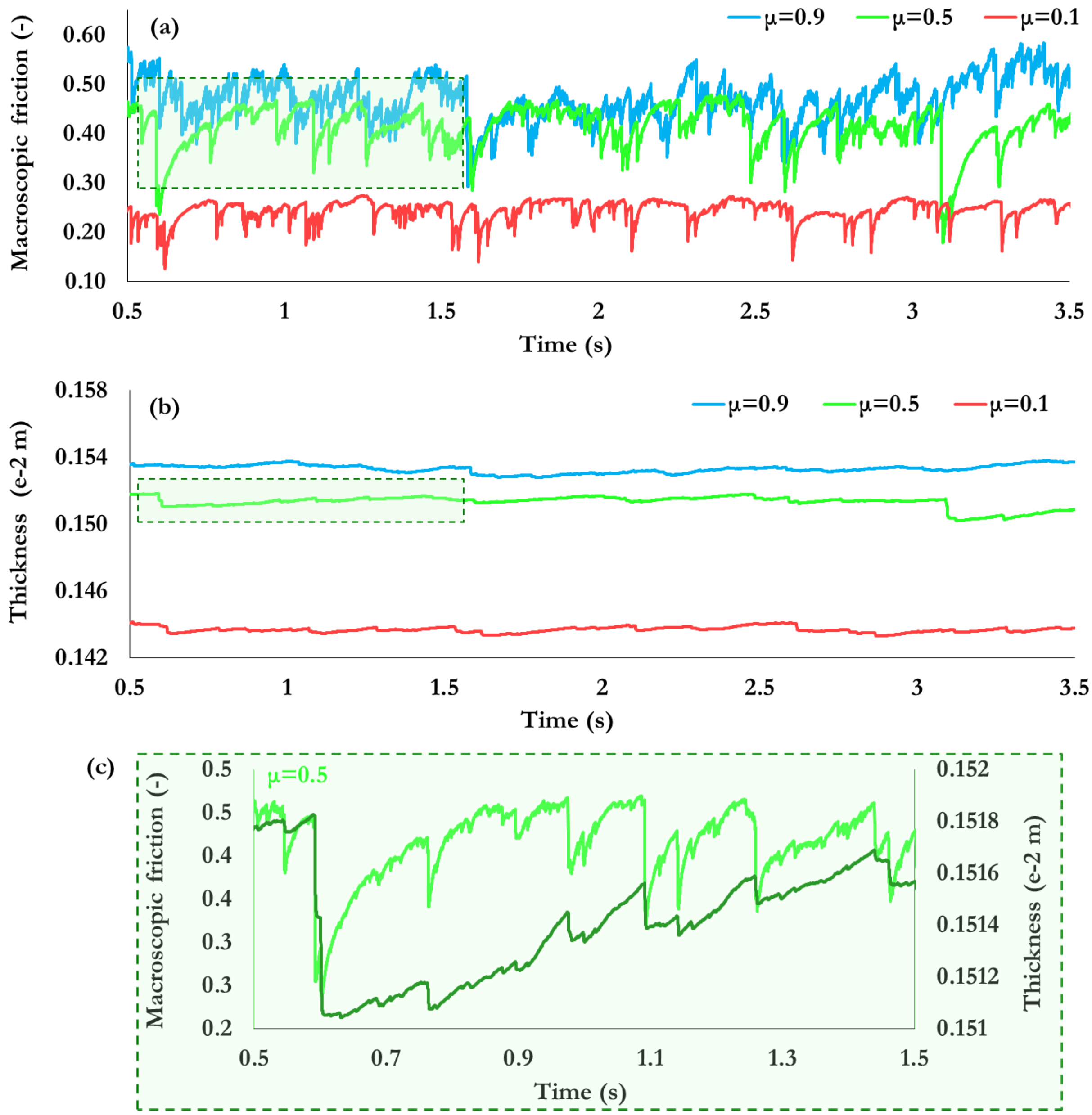

Fig. 2: Time series of (a) macroscopic friction and (b) fault gouge thickness for three different inter-particle friction coefficients. The greenish shaded areas in a and b are shown in (c) with a higher resolution for $\mu = 0.5$. Please note that the thickness is shown with a secondary axis in c.

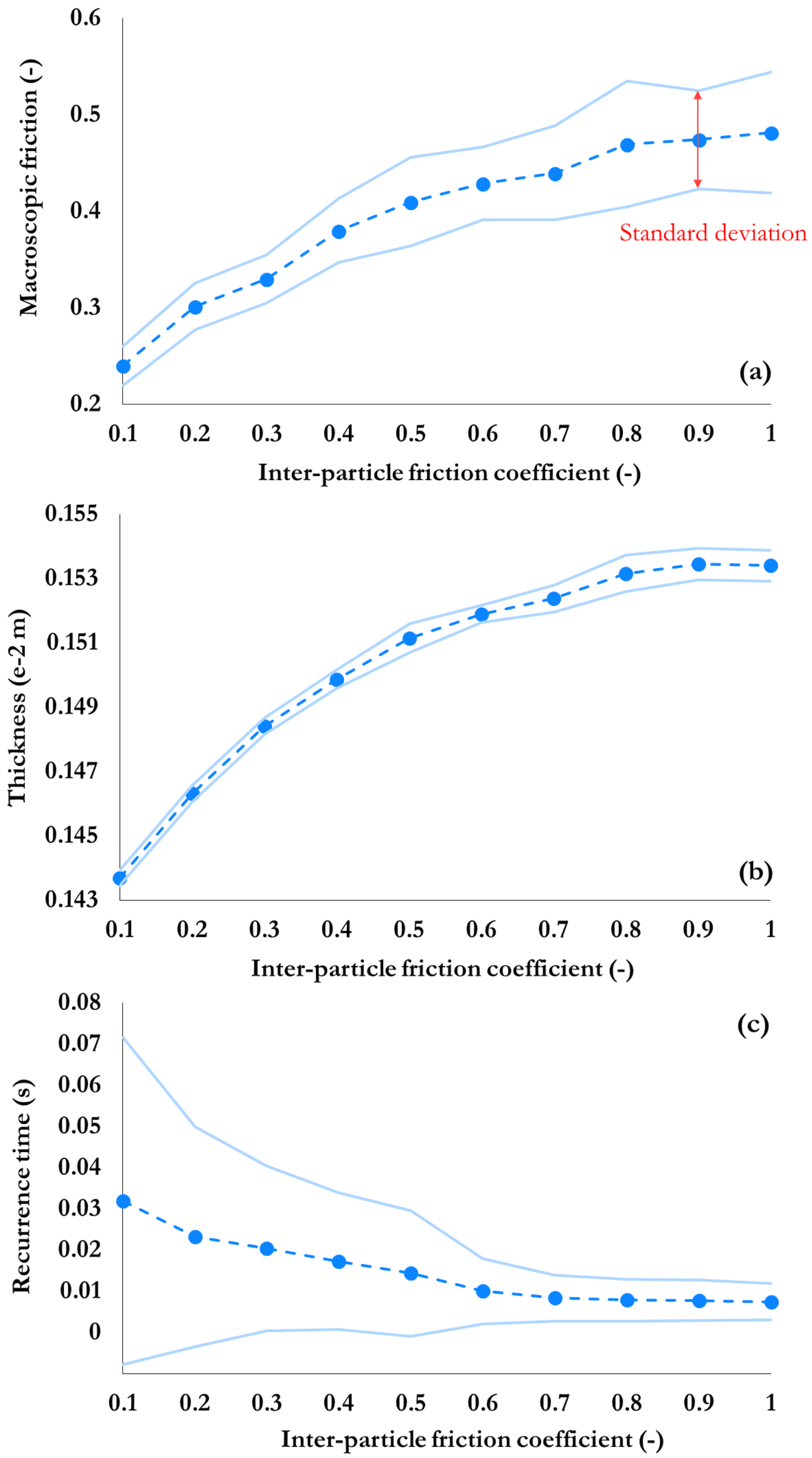

Fig. 3: Average (a) macroscopic friction, (b) fault gouge thickness and (c) slip recurrence time for long time-train stick-slip dynamics as function of the inter-particle friction coefficient. The light blue line in each image shows the uncertainty limits based on the standard deviation of data.

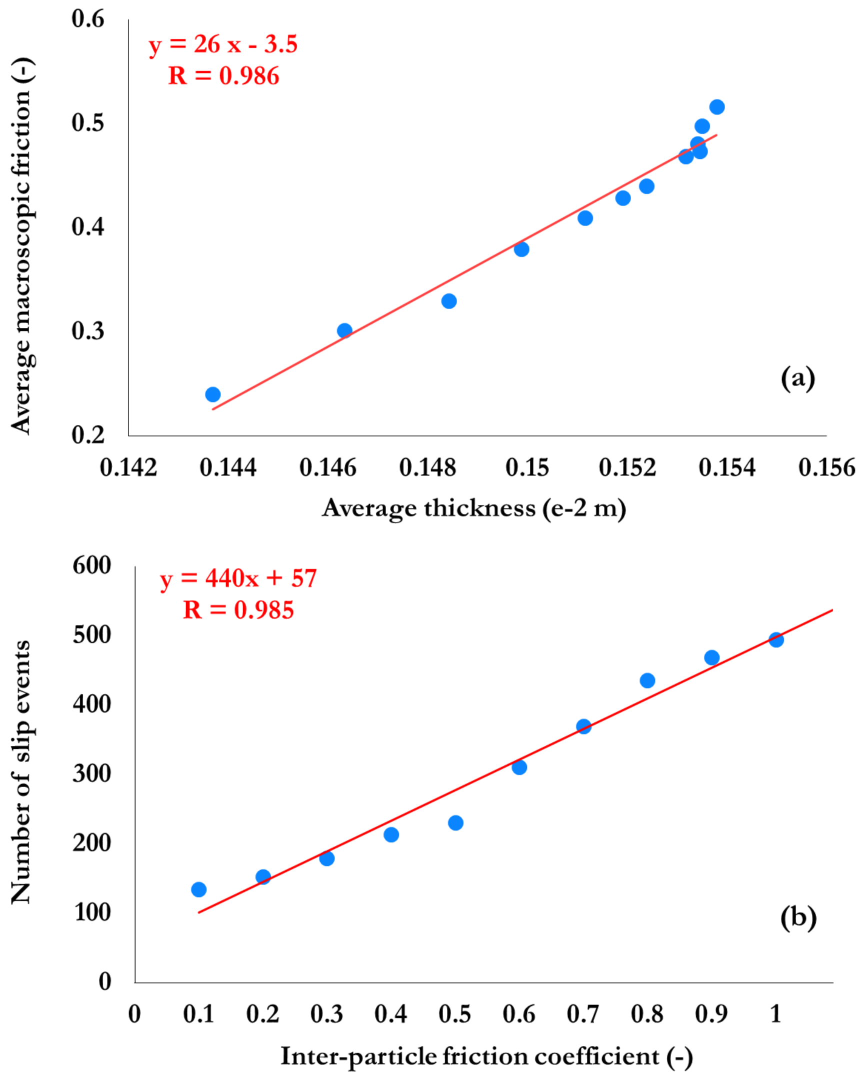

Fig. 4: (a) Average macroscopic friction versus average thickness for stick-slip dynamics with different inter-particle friction coefficients. (b) Number of slip events versus inter-particle friction coefficient.

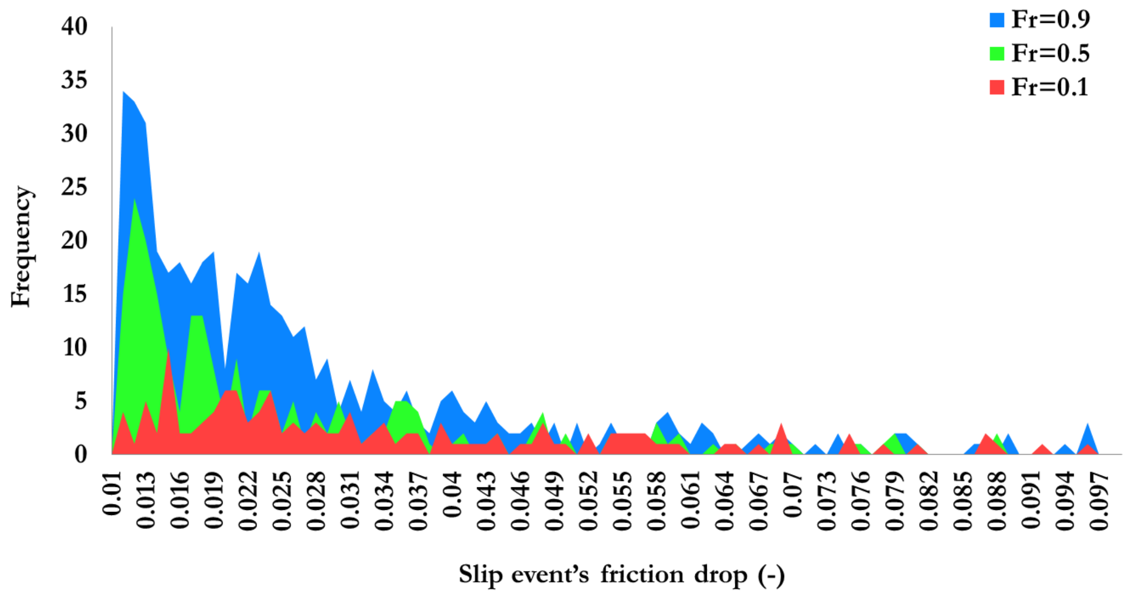

Fig. 5: Histogram of slip event's friction drop for three different inter-particle friction coefficients. The maximum slip event's friction drop in this histogram is limited to 0.1 to highlight and better show the frequency of slip events with small friction drop.

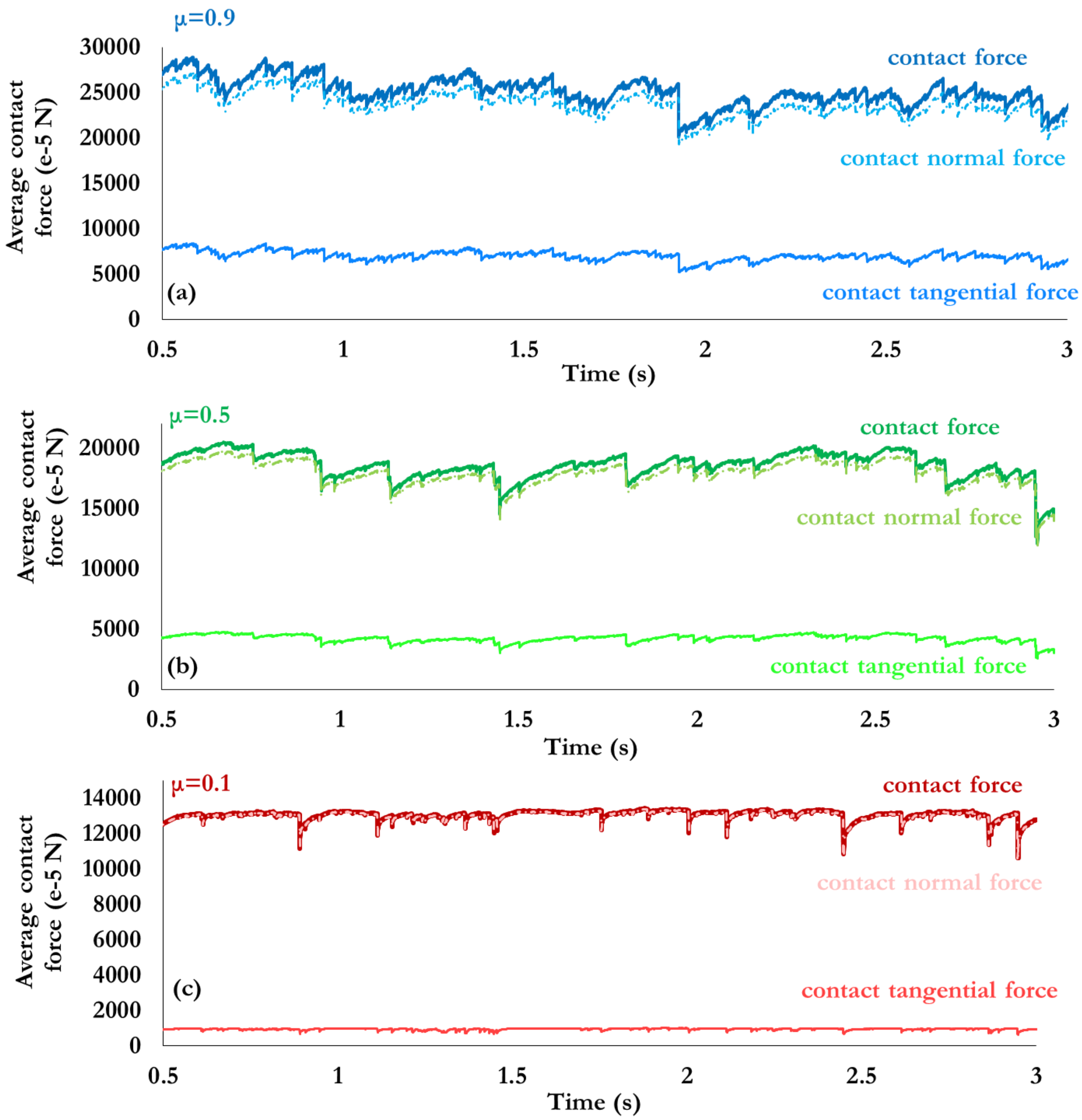

Fig. 6: (a-c) Average contact force for inter-particle friction coefficients of 0.1, 0.5 and 0.9, respectively. In each panel, the components of contact force (normal contact force and tangential contact force) are separately shown.

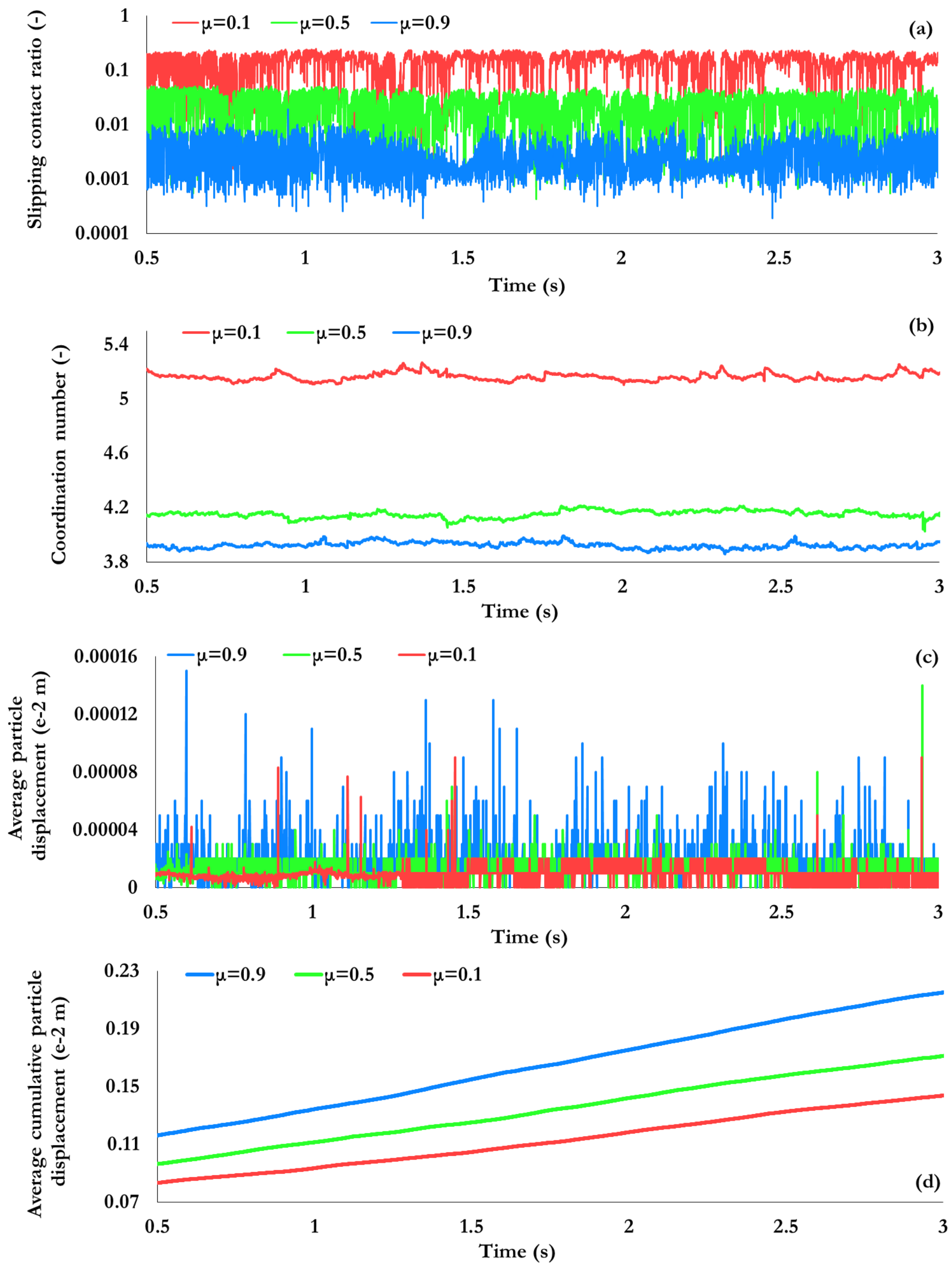

Fig. 7: Time series of (a) slipping contact ratio, (b) coordination number, (c) average particle displacement and (c) average cumulative particle displacement for inter-particle friction coefficients of 0.1, 0.5 and 0.9.

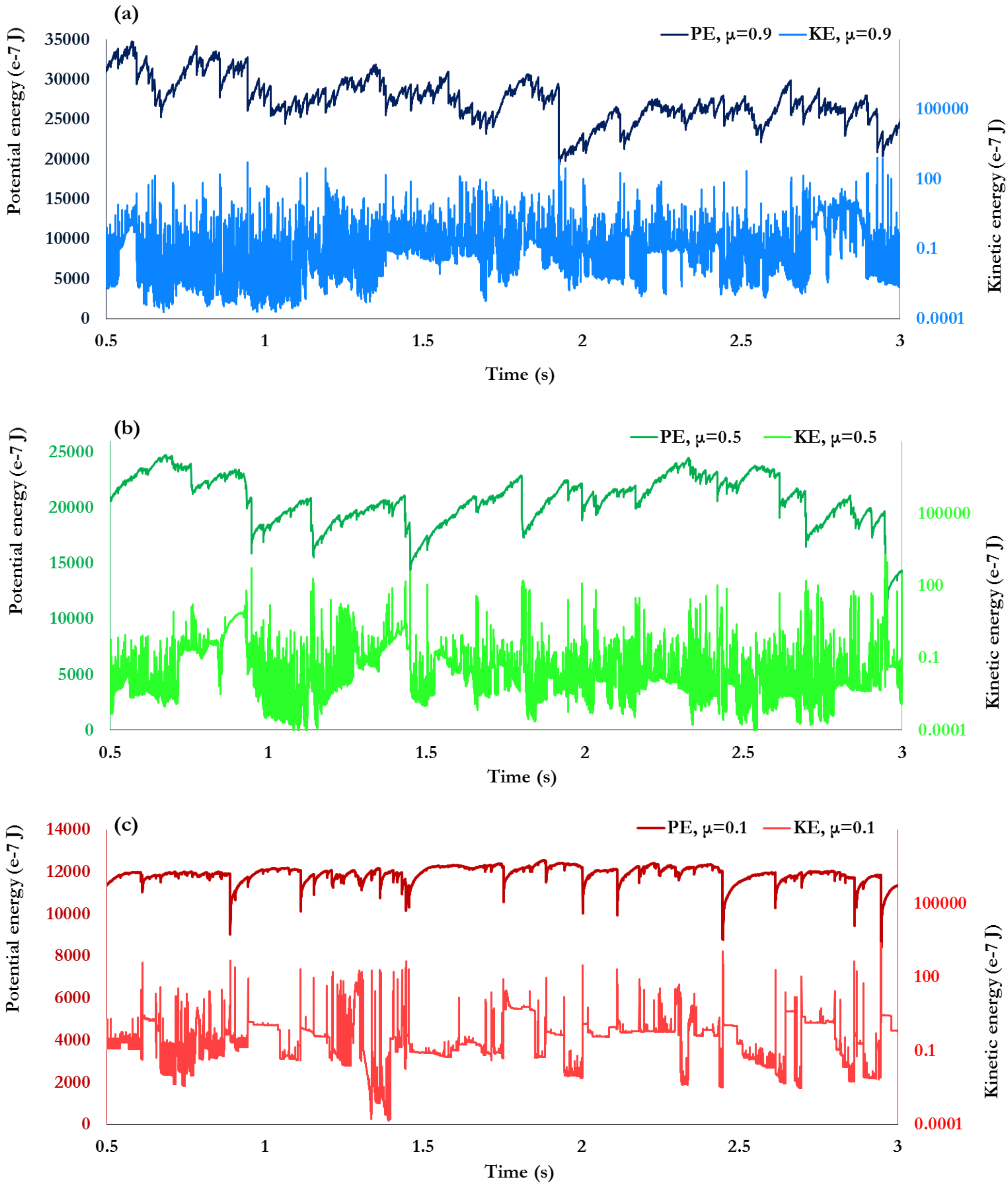

Fig. 8: (a-c) Evolution of potential energy (primary axis, left) and kinetic energy (secondary logarithmic axis, right) for inter-particle friction coefficients of 0.9, 0.5 and 0.1, respectively.

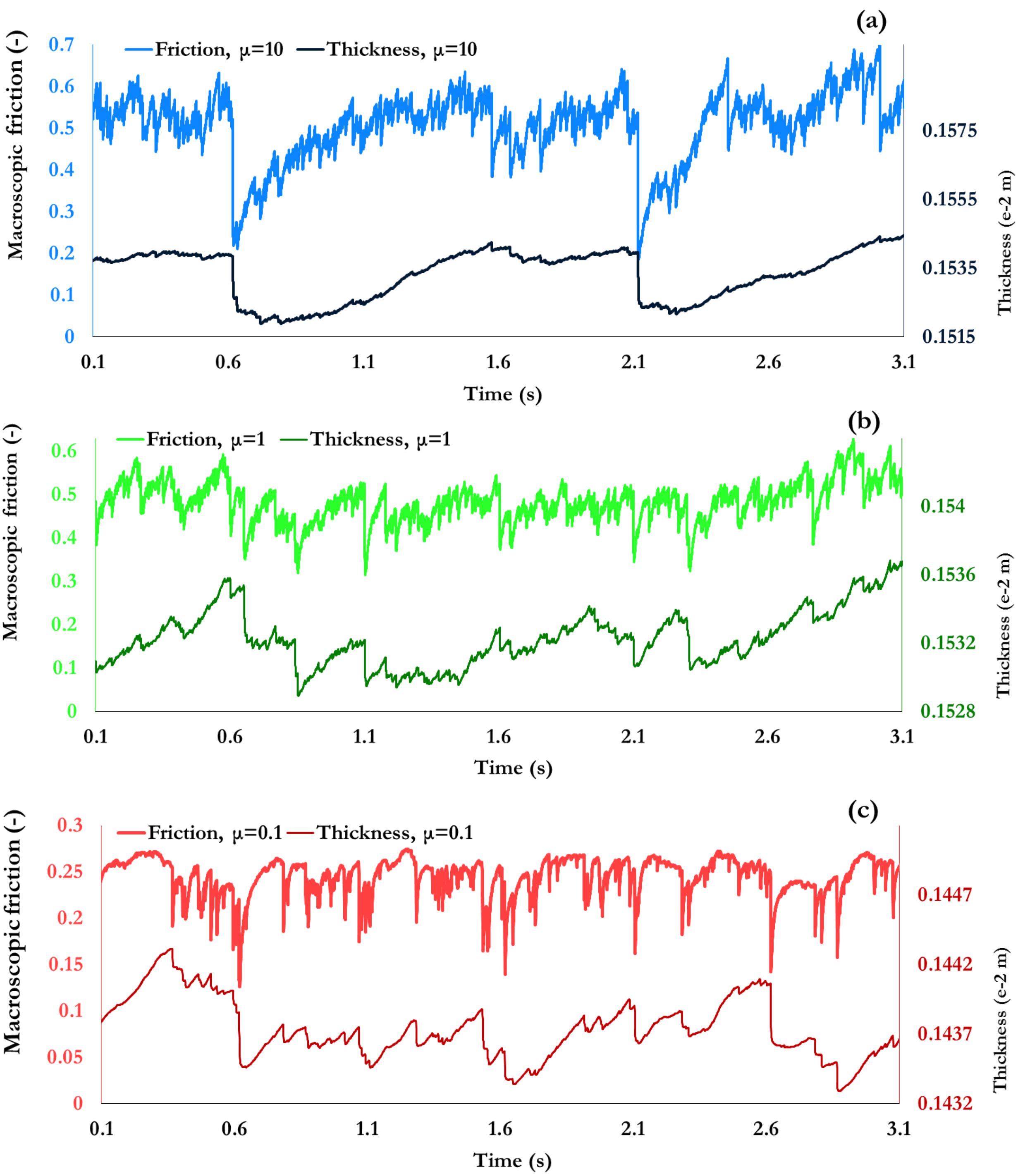

Fig. 9: (a-c) Time series of macroscopic friction (primary axis, left) and gouge thickness (secondary axis, right) for inter-particle friction coefficients of 10, 1, 0.1 respectively.

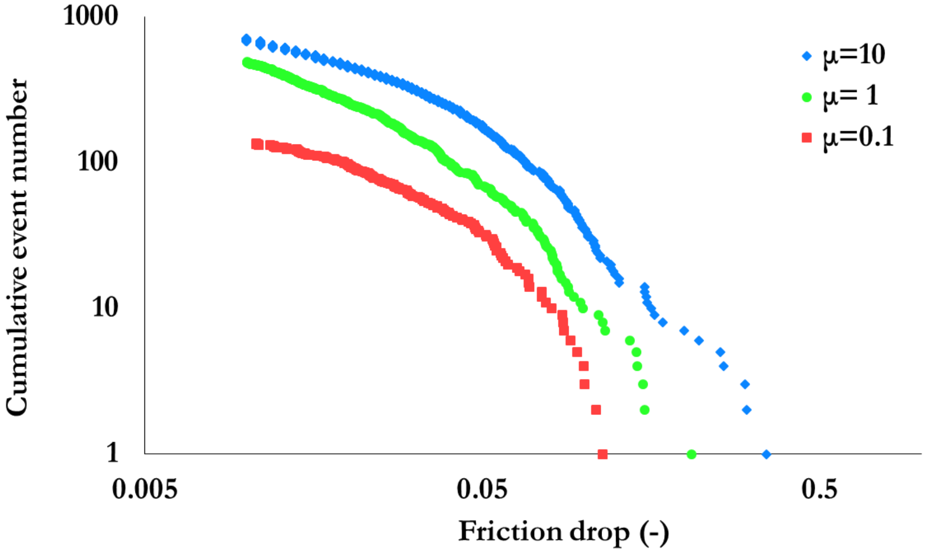

Fig. 10: Cumulative number of slip events versus friction coefficient drop for different inter-particle friction coefficients of 10, 1 and 0.1.

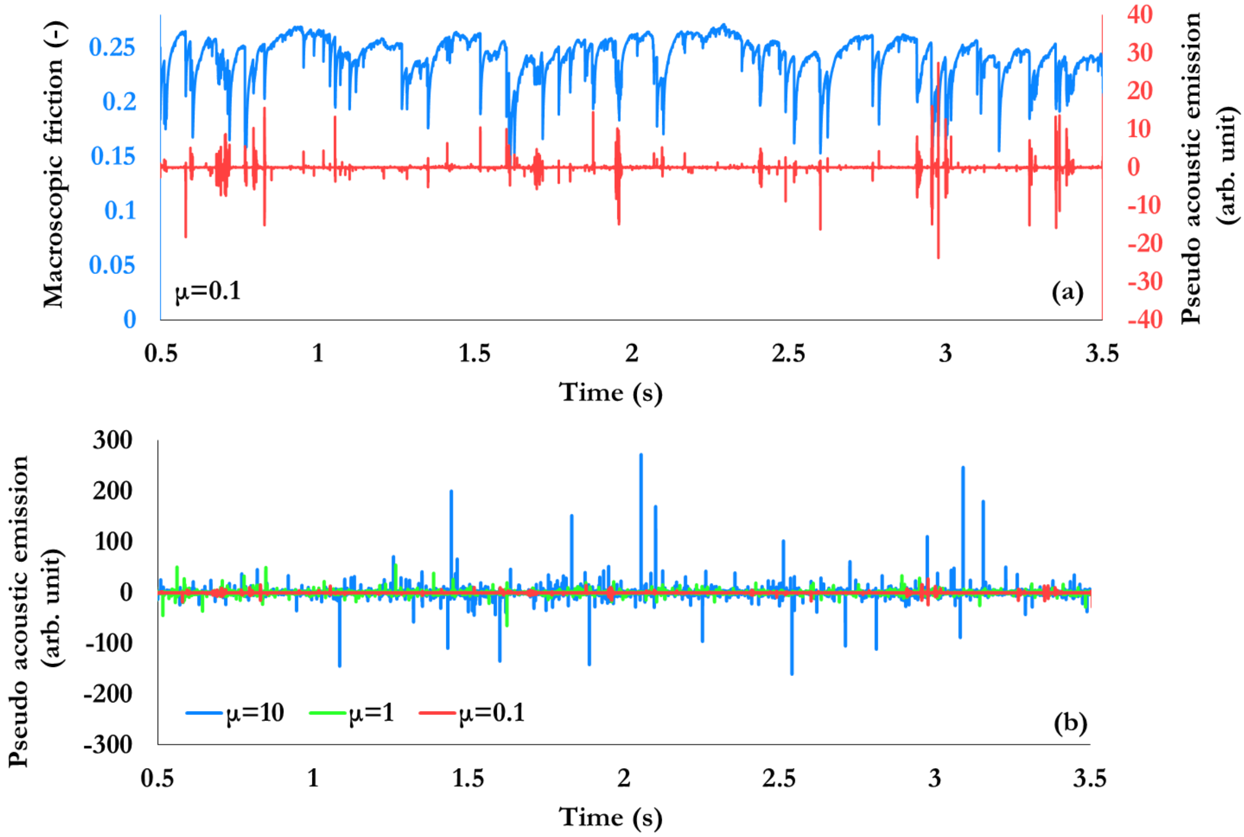

Fig. 11: (a) Friction coefficient (primary axis, left) and pseudo acoustic emission (secondary axis, right) for inter-particle friction coefficients of 10, 1 and 0.1. (b) Time series of pseudo acoustic emission for inter-particle friction coefficients of 10, 1 and 0.1.

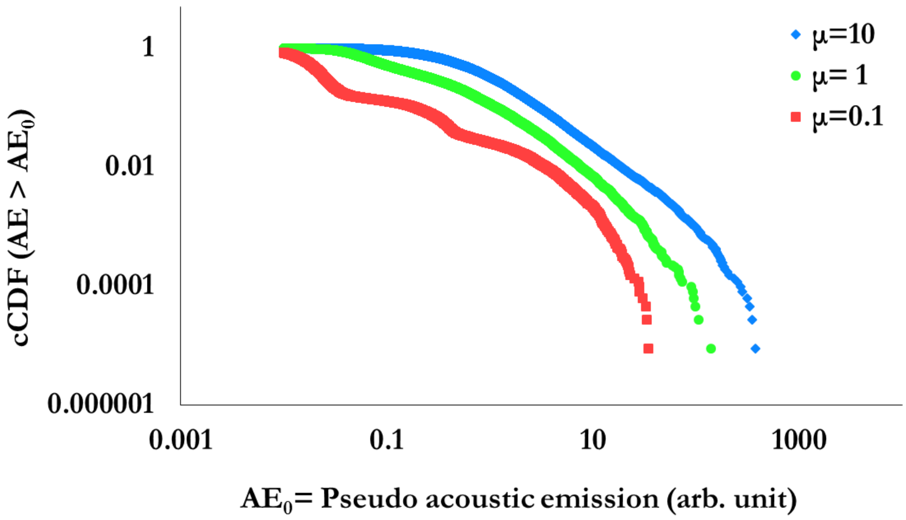

Fig. 12: Complementary Cumulative Distribution Function of pseudo acoustic emission for different inter-particle friction coefficients of 10, 1 and 0.1.

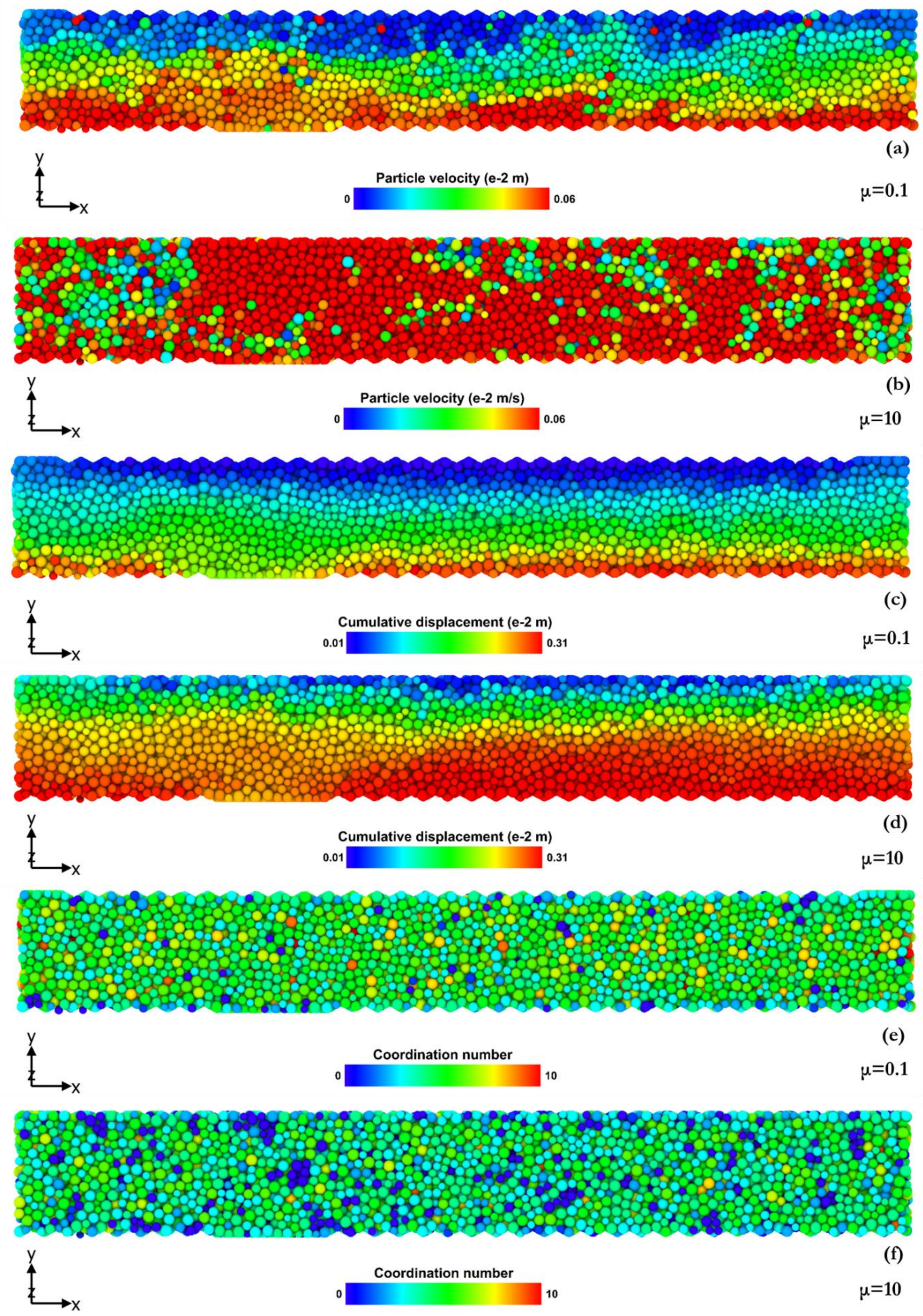

Fig. 13: (a, c, e) Spatial distribution of particle velocity, cumulative displacement and coordination number for inter-particle friction coefficients of 0.1 and (b, d, f) for inter-particle friction coefficient of 10, respectively.

8- References

Agnolin, I., & Roux, J. N. (2007). Internal states of model isotropic granular packings. I. Assembling process, geometry, and contact networks. *Phys. Rev. E, 76*(6). doi:10.1103/PhysRevE.76.061302

Angheluta, L., Candela, T., Mathiesen, J., & Renard, F. (2011). Effect of surface morphology on the dissipation during shear and slip along a rock–rock interface that contains a visco-elastic core. *Pure Appl. Geophys., 168*(12), 2335-2344. doi:10.1007/s00024-011-0272-8

Anthony, J. L., & Marone, C. (2005). Influence of particle characteristics on granular friction. *J. Geophys. Res., 110*(B8). doi:10.1029/2004jb003399

Azéma, E., Estrada, N., Preechawuttipong, I., Delenne, J.-Y., & Radjai, F. (2017). Systematic description of the effect of particle shape on the strength properties of granular media. *EPJ Web Conf., 140*, 06026.

Azéma, E., Estrada, N., & Radjaï, F. (2012). Nonlinear effects of particle shape angularity in sheared granular media. *Phys. Rev. E, 86*(4), 041301. doi:10.1103/PhysRevE.86.041301

Biegel, R. L., Sammis, C. G., & Dieterich, J. H. (1989). The frictional properties of a simulated gouge having a fractal particle distribution. *J. Struct. Geol., 11*(7), 827-846. doi:https://doi.org/10.1016/0191-8141(89)90101-6

Bistacchi, A., Griffith, W. A., Smith, S. A. F., Di Toro, G., Jones, R., & Nielsen, S. (2011). Fault roughness at seismogenic depths from lidar and photogrammetric analysis. *Pure Appl. Geophys., 168*(12), 2345-2363. doi:10.1007/s00024-011-0301-7

Bouchon, M., Karabulut, H., Bouin, M.-P., Schmittbuhl, J., Vallée, M., Archuleta, R., . . . Marsan, D. (2010). Faulting characteristics of supershear earthquakes. *Tectonophysics, 493*(3), 244-253. doi:https://doi.org/10.1016/j.tecto.2010.06.011

Brantut, N., Schubnel, A., Rouzaud, J. N., Brunet, F., & Shimamoto, T. (2008). High-velocity frictional properties of a clay-bearing fault gouge and implications for earthquake mechanics. *J. Geophys. Res., 113*(B10). doi:10.1029/2007JB005551

Brodsky, E. E., Gilchrist, J. J., Sagy, A., & Collettini, C. (2011). Faults smooth gradually as a function of slip. *Earth Planet. Sci. Lett., 302*(1), 185-193. doi:https://doi.org/10.1016/j.epsl.2010.12.010

Brodsky, E. E., Kirkpatrick, J. D., & Candela, T. (2016). Constraints from fault roughness on the scale-dependent strength of rocks. *Geology, 44*(1), 19-22.

Bruhat, L., Fang, Z., & Dunham, E. M. (2016). Rupture complexity and the supershear transition on rough faults. *J. Geophys. Res., 121*(1), 210-224. doi:doi:10.1002/2015JB012512

Candela, T., Renard, F., Bouchon, M., Brouste, A., Marsan, D., Schmittbuhl, J., & Voisin, C. (2009). Characterization of fault roughness at various scales: Implications of three-dimensional high resolution topography measurements. *Pure Appl. Geophys., 166*(10), 1817-1851. doi:10.1007/s00024-009-0521-2

Candela, T., Renard, F., Bouchon, M., Schmittbuhl, J., & Brodsky, E. E. (2011a). Stress drop during earthquakes: Effect of fault roughness scaling. *Bull. Seismol. Soc. Am., 101*(5), 2369-2387.

Candela, T., Renard, F., Klinger, Y., Mair, K., Schmittbuhl, J., & Brodsky, E. E. (2012). Roughness of fault surfaces over nine decades of length scales. *J. Geophys. Res., 117*(B8). doi:doi:10.1029/2011JB009041

Candela, T., Renard, F., Schmittbuhl, J., Bouchon, M., & Brodsky, E. E. (2011b). Fault slip distribution and fault roughness. *Geophys. J. Int., 187*(2), 959-968. doi:10.1111/j.1365-246X.2011.05189.x

Cashman, S., & Cashman, K. (2000). Cataclasis and deformation-band formation in unconsolidated marine terrace sand, humboldt county, california. *Geology, 28*(2), 111-114. doi:10.1130/0091-7613(2000)28<111:CADFIU>2.0.CO;2

Cashman, S. M., Baldwin, J. N., Cashman, K. V., Swanson, K., & Crawford, R. (2007). Microstructures developed by coseismic and aseismic faulting in near-surface sediments, san andreas fault, california. *Geology, 35*(7), 611-614.

Chester, F. M., & Chester, J. S. (1998). Ultracataclasite structure and friction processes of the punchbowl fault, san andreas system, california. *Tectonophysics, 295*(1), 199-221. doi:https://doi.org/10.1016/S0040-1951(98)00121-8

Chester, F. M., & Chester, J. S. (2000). Stress and deformation along wavy frictional faults. *J. Geophys. Res., 105*(B10), 23421-23430. doi:doi:10.1029/2000JB900241

Chester, F. M., Friedman, M., & Logan, J. M. (1985). Foliated cataclasites. *Tectonophysics, 111*(1), 139-146. doi:https://doi.org/10.1016/0040-1951(85)90071-X

Chester, F. M., & Logan, J. M. (1986). Implications for mechanical properties of brittle faults from observations of the punchbowl fault zone, california. *Pure Appl. Geophys., 124*(1), 79-106. doi:10.1007/bf00875720

Di Renzo, A., & Di Maio, F. P. (2004). Comparison of contact-force models for the simulation of collisions in dem-based granular flow codes. *Chem. Eng. Sci., 59*(3), 525-541. doi:10.1016/j.ces.2003.09.037

Dieterich, J. H., & Kilgore, B. D. (1994). Direct observation of frictional contacts: New insights for state-dependent properties. *Pure Appl. Geophys., 143*(1), 283-302. doi:10.1007/bf00874332

Dieterich, J. H., & Smith, D. E. (2009). Nonplanar faults: Mechanics of slip and off-fault damage. *Pure Appl. Geophys., 166*(10), 1799-1815. doi:10.1007/s00024-009-0517-y

Dorostkar, O. (2018). *Stick-slip dynamics in dry and fluid saturated granular fault gouge investigated by numerical simulations.* (PhD dissertaion), PhD dissertaion, ETH Zurich.

Dorostkar, O., & Carmeliet, J. (2018). Potential energy as metric for understanding stick–slip dynamics in sheared granular fault gouge: A coupled cfd–dem study. *Rock Mech. Rock Eng.* doi:10.1007/s00603-018-1457-6

Dorostkar, O., Guyer, R. A., Johnson, P. A., Marone, C., & Carmeliet, J. (2017a). On the micromechanics of slip events in sheared, fluid saturated fault gouge. *Geophys. Res. Lett.*, 6101–6108. doi:10.1002/2017GL073768

Dorostkar, O., Guyer, R. A., Johnson, P. A., Marone, C., & Carmeliet, J. (2017b). On the role of fluids in stick-slip dynamics of saturated granular fault gouge using a coupled computational fluid dynamics-discrete element approach. *J. Geophys. Res.* doi:10.1002/2017JB014099

Dorostkar, O., Guyer, R. A., Johnson, P. A., Marone, C., & Carmeliet, J. (2018). Cohesion-induced stabilization in stick-slip dynamics of weakly wet, sheared granular fault gouge. *J. Geophys. Res.* doi:10.1002/2017JB015171

Dorostkar, O., Johnson, P., Guyer, R., Marone, C., & Carmeliet, J. (2017c). Do fluids modify the stick-slip behavior of sheared granular media? *Poromechanics VI : Proceedings of the Sixth Biot Conference on Poromechanics, 2017.* , 158-163. doi:10.1061/9780784480779.019

Dunham, E. M., Belanger, D., Cong, L., & Kozdon, J. E. (2011). Earthquake ruptures with strongly rate-weakening friction and off-fault plasticity, part 2: Nonplanar faults. *Bull. Seismol. Soc. Am., 101*(5), 2308-2322.

Engelder, J. T. (1974). Cataclasis and the generation of fault gouge. *GSA Bulletin, 85*(10), 1515-1522. doi:10.1130/0016-7606(1974)85<1515:CATGOF>2.0.CO;2

Faulkner, D. R., Lewis, A. C., & Rutter, E. H. (2003). On the internal structure and mechanics of large strike-slip fault zones: Field observations of the carboneras fault in southeastern spain. *Tectonophysics, 367*(3), 235-251. doi:https://doi.org/10.1016/S0040-1951(03)00134-3

Ferdowsi, B. (2014). *Discrete element modeling of triggered slip in faults with granular gouge: Application to dynamic earthquake triggering.* (PhD dissertaion), ETH Zurich.

Fournier, T., & Morgan, J. (2012). Insights to slip behavior on rough faults using discrete element modeling. *Geophys. Res. Lett., 39*(12). doi:doi:10.1029/2012GL051899

Frye, K. M., & Marone, C. (2002). Effect of humidity on granular friction at room temperature. *J. Geophys. Res., 107*(B11). doi:10.1029/2001jb000654

Goebel, T. H. W., Becker, T. W., Sammis, C. G., Dresen, G., & Schorlemmer, D. (2014a). Off-fault damage and acoustic emission distributions during the evolution of structurally complex faults over series of stick-slip events. *Geophys. J. Int., 197*(3), 1705-1718. doi:10.1093/gji/ggu074

Goebel, T. H. W., Becker, T. W., Schorlemmer, D., Stanchits, S., Sammis, C., Rybacki, E., & Dresen, G. (2012). Identifying fault heterogeneity through mapping spatial anomalies in acoustic emission statistics. *J. Geophys. Res., 117*(B3). doi:doi:10.1029/2011JB008763

Goebel, T. H. W., Candela, T., Sammis, C. G., Becker, T. W., Dresen, G., & Schorlemmer, D. (2014b). Seismic event distributions and off-fault damage during frictional sliding of saw-cut surfaces with pre-defined roughness. *Geophys. J. Int., 196*(1), 612-625. doi:10.1093/gji/ggt401

Goebel, T. H. W., Kwiatek, G., Becker, T. W., Brodsky, E. E., & Dresen, G. (2017). What allows seismic events to grow big?: Insights from b-value and fault roughness analysis in laboratory stick-slip experiments. *Geology, 45*(9), 815-818. doi:10.1130/G39147.1

Göncü, F., & Luding, S. (2013). Effect of particle friction and polydispersity on the macroscopic stress–strain relations of granular materials. *Acta Geotech., 8*(6), 629-643. doi:10.1007/s11440-013-0258-z

Goniva, C., Kloss, C., Deen, N. G., Kuipers, J. A. M., & Pirker, S. (2012). Influence of rolling friction on single spout fluidized bed simulation. *PARTICUOLOGY, 10*(5), 582-591. doi:10.1016/j.partic.2012.05.002

Haines, S., Marone, C., & Saffer, D. (2014). Frictional properties of low-angle normal fault gouges and implications for low-angle normal fault slip. *Earth Planet. Sci. Lett., 408*, 57-65. doi:10.1016/j.epsl.2014.09.034

Heermance, R., Shipton, Z. K., & Evans, J. P. (2003). Fault structure control on fault slip and ground motion during the 1999 rupture of the chelungpu fault, taiwan. *Bull. Seismol. Soc. Am., 93*(3), 1034-1050. doi:10.1785/0120010230

Hertz, H. (1882). Ueber die berührung fester elastischer körper. *Journal für die reine und angewandte Mathematik, 92*, 156-171.

Ivković, B., Djurdjanović, M., & Stamenković, D. (2000). *The influence of the contact surface roughness on the static friction coefficient* (Vol. 22).

J. Latham, S., Abe, S., & R. Mora, P. (2005). *Macroscopic friction response of rotational and non-rotational lattice solid gouge models in 2d and 3d.* Paper presented at the Powders and Grains 2005, Stuttgart, Germany.

Johnson, P. A., Ferdowsi, B., Kaproth, B. M., Scuderi, M., Griffa, M., Carmeliet, J., . . . Marone, C. (2013). Acoustic emission and microslip precursors to stick-slip failure in sheared granular material. *Geophys. Res. Lett., 40*(21), 5627-5631. doi:10.1002/2013gl057848

Johnson, P. A., & Jia, X. (2005). Nonlinear dynamics, granular media and dynamic earthquake triggering. *Nature, 437*(7060), 871-874. doi:10.1038/nature04015

Karner, S. L., & Marone, C. (2000). Effects of loading rate and normal stress on stress drop and stick-slip recurrence interval. *GeoComplexity and the Physics of Earthquakes*, 187-198.

Kloss, C., Goniva, C., Hager, A., Amberger, S., & Pirker, S. (2012). Models, algorithms and validation for opensource dem and cfd-dem. *Prog. Comput. Fluid Dy., 12*(2-3), 140-152.

Knuth, M., & Marone, C. (2007). Friction of sheared granular layers: Role of particle dimensionality, surface roughness, and material properties. *Geochem. Geophys. Geosyst., 8*(3). doi:doi:10.1029/2006GC001327

Kozłowska, M., Brudzinski, M. R., Friberg, P., Skoumal, R. J., Baxter, N. D., & Currie, B. S. (2018). Maturity of nearby faults influences seismic hazard from hydraulic fracturing. *Proceedings of the National Academy of Sciences, 115*(8), E1720-E1729. doi:10.1073/pnas.1715284115

Kwiatek, G., Goebel, T. H. W., & Dresen, G. (2014). Seismic moment tensor and b value variations over successive seismic cycles in laboratory stick-slip experiments. *Geophys. Res. Lett., 41*(16), 5838-5846. doi:doi:10.1002/2014GL060159

Leeman, J. R., Saffer, D. M., Scuderi, M. M., & Marone, C. (2016). Laboratory observations of slow earthquakes and the spectrum of tectonic fault slip modes. *Nat Commun, 7*, 11104. doi:10.1038/ncomms11104

https://www.nature.com/articles/ncomms11104#supplementary-information

Mair, K., Frye, K. M., & Marone, C. (2002). Influence of grain characteristics on the friction of granular shear zones. *J. Geophys. Res., 107*(B10). doi:10.1029/2001jb000516

Makedonska, N., Sparks, D. W., Aharonov, E., & Goren, L. (2011). Friction versus dilation revisited: Insights from theoretical and numerical models. *J. Geophys. Res., 116*(B9). doi:10.1029/2010jb008139

Marone, C. (1998a). The effect of loading rate on static friction and the rate of fault healing during the earthquake cycle. *Nature, 391*(6662), 69-72. doi:10.1038/34157

Marone, C. (1998b). Laboratory-derived friction laws and their application to seismic faulting. *Annu. Rev. Earth Planet. Sci., 26*, 643-696. doi:10.1146/annurev.earth.26.1.643

Marone, C., Carpenter, B. M., & Schiffer, P. (2008). Transition from rolling to jamming in thin granular layers. *Physical Review Letters, 101*(24), 248001.

Marone, C., & Kilgore, B. (1993). Scaling of the critical slip distance for seismic faulting with shear strain in fault zones. *Nature, 362*, 618. doi:10.1038/362618a0

Marone, C., Raleigh, C. B., & Scholz, C. H. (1990). Frictional behavior and constitutive modeling of simulated fault gouge. *J. Geophys. Res., 95*(B5), 7007-7025. doi:10.1029/JB095iB05p07007

McLaskey, G. C., & Glaser, S. D. (2011). Micromechanics of asperity rupture during laboratory stick slip experiments. *Geophys. Res. Lett., 38*(12). doi:doi:10.1029/2011GL047507

Mead, W. J. (1925). The geologic role of dilatancy. *The Journal of Geology, 33*(7), 685-698.

MiDi, G. D. R. (2004). On dense granular flows. *Eur. Phys. J. E, 14*(4), 341-365. doi:10.1140/epje/i2003-10153-0

O'Sullivan, C. (2011). *Particulate discrete element modelling: A geomechanics perspective*: Spon Press.

Ohnaka, M. (2003). A constitutive scaling law and a unified comprehension for frictional slip failure, shear fracture of intact rock, and earthquake rupture. *J. Geophys. Res., 108*(B2). doi:doi:10.1029/2000JB000123

Ohnaka, M., & Shen, L.-f. (1999). Scaling of the shear rupture process from nucleation to dynamic propagation: Implications of geometric irregularity of the rupturing surfaces. *J. Geophys. Res., 104*(B1), 817-844. doi:doi:10.1029/1998JB900007

Park, J.-W., & Song, J.-J. (2009). Numerical simulation of a direct shear test on a rock joint using a bonded-particle model. *Int. J. Rock Mech. Min. Sci., 46*(8), 1315-1328. doi:https://doi.org/10.1016/j.ijrmms.2009.03.007

Pierre, R., S., B. H., Romain, J., & Raúl, M. (2018). Fast and slow slip events emerge due to fault geometrical complexity. *Geophys. Res. Lett., 45*(10), 4809-4819. doi:doi:10.1029/2018GL077579

Rabinowicz, E. (1956). Stick and slip. *Sci. Am., 194*(5), 109-119.

Rathbun, A. P., & Marone, C. (2010). Effect of strain localization on frictional behavior of sheared granular materials. *J. Geophys. Res., 115*(B1). doi:10.1029/2009jb006466

Rathbun, A. P., Renard, F., & Abe, S. (2013). Numerical investigation of the interplay between wall geometry and friction in granular fault gouge. *J. Geophys. Res., 118*(3), 878-896. doi:doi:10.1002/jgrb.50106

Renard, F., & Candela, T. (2017). Scaling of fault roughness and implications for earthquake mechanics *Fault zone dynamic processes: Evolution of fault properties during seismic rupture, geophysical monograph 227*: John Wiley & Sons, Inc.

Renard, F., Voisin, C., Marsan, D., & Schmittbuhl, J. (2006). High resolution 3d laser scanner measurements of a strike-slip fault quantify its morphological anisotropy at all scales. *Geophys. Res. Lett., 33*(4). doi:doi:10.1029/2005GL025038

Rijsingen, E., Lallemand, S., Peyret, M., Arcay, D., Heuret, A., Funiciello, F., & Corbi, F. (2018). How subduction interface roughness influences the occurrence of large interplate earthquakes. *Geochem. Geophys. Geosyst.* doi:doi:10.1029/2018GC007618

Rivière, J., Lv, Z., Johnson, P. A., & Marone, C. (2018). Evolution of b-value during the seismic cycle: Insights from laboratory experiments on simulated faults. *Earth Planet. Sci. Lett., 482*, 407-413. doi:https://doi.org/10.1016/j.epsl.2017.11.036

Rosenau, M., Corbi, F., & Dominguez, S. (2017). Analogue earthquakes and seismic cycles: Experimental modelling across timescales. *Solid Earth, 8*(3), 597-635. doi:10.5194/se-8-597-2017

Rouet-Leduc, B., Hulbert, C., Lubbers, N., Barros, K., Humphreys, C. J., & Johnson, P. A. (2017). Machine learning predicts laboratory earthquakes. *Geophys. Res. Lett., 44*(18), 9276-9282. doi:10.1002/2017GL074677

Sagy, A., Brodsky, E. E., & Axen, G. J. (2007). Evolution of fault-surface roughness with slip. *Geology, 35*(3), 283-286. doi:10.1130/G23235A.1

Schubnel, A., Nielsen, S., Taddeucci, J., Vinciguerra, S., & Rao, S. (2011). Photo-acoustic study of subshear and supershear ruptures in the laboratory. *Earth Planet. Sci. Lett., 308*(3), 424-432. doi:https://doi.org/10.1016/j.epsl.2011.06.013

Sheng, Y., Lawrence, C. J., Briscoe, B. J., & Thornton, C. (2004). Numerical studies of uniaxial powder compaction process by 3d dem. *Eng. Computation., 21*(2-4), 304-317. doi:10.1108/02644400410519802

Shimamoto, T. (1979). *Experimental studies of simulated gouge and their application to studies of natural fault zones*. Paper presented at the Conference VIII: Analysis of Actual Fault Zones in Bedrock, Natl. Earthquake Hazards Reduct. Program, Menlo Park, Calif.

Shojaaee, Z., Brendel, L., Török, J., & Wolf, D. E. (2012). Shear flow of dense granular materials near smooth walls. Ii. Block formation and suppression of slip by rolling friction. *Phys. Rev. E, 86*(1), 011302. doi:10.1103/PhysRevE.86.011302

Tal, Y., & Hager, B. H. (2018). The slip behavior and source parameters for spontaneous slip events on rough faults subjected to slow tectonic loading. *J. Geophys. Res., 123*(2), 1810-1823. doi:doi:10.1002/2017JB014737

Tal, Y., Hager, B. H., & Ampuero, J. P. (2018). The effects of fault roughness on the earthquake nucleation process. *J. Geophys. Res., 123*(1), 437-456. doi:doi:10.1002/2017JB014746

Wang, K., & Bilek, S. L. (2014). Invited review paper: Fault creep caused by subduction of rough seafloor relief. *Tectonophysics, 610*, 1-24. doi:https://doi.org/10.1016/j.tecto.2013.11.024

Wang, W.-J., Kong, X.-Z., & Zhu, Z.-G. (2007). Friction and relative energy dissipation in sheared granular materials. *Phys. Rev. E, 75*(4), 041302.

Xia, K., Rosakis, A. J., & Kanamori, H. (2004). Laboratory earthquakes: The sub-rayleigh-to-supershear rupture transition. *Science, 303*(5665), 1859-1861. doi:10.1126/science.1094022

Zielke, O., Galis, M., & Mai, P. M. (2017). Fault roughness and strength heterogeneity control earthquake size and stress drop. *Geophys. Res. Lett., 44*(2), 777-783. doi:doi:10.1002/2016GL071700

Zoback, M., Hickman, S., & Ellsworth, W. (2010). Scientific drilling into the san andreas fault zone. *Eos, Transactions American Geophysical Union, 91*(22), 197-199.